Rock Mech Rock Eng (2014) 47:2021–2029
DOI 10.1007/s00603-013-0508-2

ORIGINAL PAPER

Plane Strain Testing with Passive Restraint

Roman Makhnenko · Joseph Labuz

Received: 26 August 2013 / Accepted: 28 October 2013 / Published online: 19 November 2013

Abstract A plane strain condition for testing rock is developed through passive restraint in the form of a thick-walled cylinder. The so-called biaxial frame generates the intermediate principal stress that imposes a triaxial state of stress on a prismatic specimen. Major and minor principal stresses and corresponding strains are accurately measured, providing data to calculate the elastic (Young's modulus and Poisson's ratio), inelastic (dilatancy angle), and strength (friction angle and cohesion) parameters of the rock. Results of experiments conducted on Indiana limestone in plane strain compression are compared with the results of axisymmetric compression and extension. With proper system calibration, Young's modulus and Poisson's ratio are consistent among the tests. The plane strain apparatus enforces in-plane deformation with the three principal stresses at failure being different, and it allows one to determine the Paul-Mohr-Coulomb failure surface, which includes an intermediate stress effect.

Keywords Plane strain testing · Passive restraint · Dilatancy · Paul-Mohr-Coulomb failure surface · Intermediate stress effect

1 Introduction

Axisymmetric or "conventional" triaxial testing if often used to determine the elastic and inelastic response of rock, as well as to measure strength characteristics, e.g., friction angle and cohesion (Jaeger et al. 2007). However, questionable predictions may arise when data obtained from axisymmetric tests are applied to two-dimensional models, specifically those simulating behavior of structures in plane strain. In addition, a number of in situ stress measurements show that principal stresses underground are often not equal (cf. Haimson 1978). Thus, in the investigation of rock failure, the intermediate principal stress effect should be considered (Mogi 1967). A number of true triaxial testing apparatus for rock have been developed in recent years (Wawersik et al. 1997; Haimson and Chang 2000; Bésuelle and Hall 2011), and these devices rely on some type of actuator applying the intermediate principal stress. It should be noted that plane strain systems using an active component (a force applied to eliminate displacement) were used in research laboratories of soil mechanics for some time (Kjellman 1936; Leussink and Wittke 1963; Cornforth 1964; Henkel and Wade 1966; Al-Hussaini 1968).

Another approach to plane strain testing is through passive restraint, where a stiff structure is used to restrict displacement in one direction (Marsal et al. 1967; Campanella and Vaid 1973). A passive device for soil designed by Smith (1963) and modified by Duncan and See (1966) relied on bar-type, axial restraint to restrict deformation; for material such as soil with Young's modulus in the order of MPa, the stiffness requirements of the bars were modest. A clever passive restraint device, also for testing soil, was built by Vardoulakis and Goldscheider (1981). A unique feature of the device was the inclusion of a linear bearing; once deformation localized, the loading platen translated and valuable information was still obtained into the post-peak region with no system interaction (Drescher et al. 1990).

The University of Minnesota plane strain apparatus (Labuz et al. 1996) is a passive restraint system for testing rock that uses an instrumented thick-walled cylinder called

R. Makhnenko (✉) · J. Labuz
Department of Civil Engineering, University of Minnesota-Twin Cities, Minneapolis, MN 55455, USA
e-mail: makhn002@umn.edu

a biaxial frame, which allows the intermediate stress to be measured with proper calibration and assumed linear response. The biaxial frame is sized to ensure that the deformation in the direction of plane strain is below a tolerable amount, e.g., one percent of the axial strain. An advantage of a plane strain apparatus is the measurement of in-plane displacements, providing accurate data for determining deformation (shear strain and volume strain) response, and the calculation of elastic and inelastic material parameters.

2 Passive Restraint

2.1 Biaxial Frame

Passive restraint for the University of Minnesota plane strain apparatus is developed by a thick-walled cylinder (Fig. 1) of mild steel called a biaxial frame, which has no seams or interfaces to provide maximum stiffness (Labuz et al. 1996). The outside diameter is 300 mm, and the inside diameter is 110 mm; based on a three-dimensional finite element analysis, the out-of-plane strain is about one percent of the axial strain for a rock with Young's modulus $E = 15$ GPa and cross-sectional area $A^s = 2{,}250$ mm^2. A circular opening with "flats" (chords of the circular opening) provides precise alignment of the prismatic specimen (Fig. 1). A pair of wedges and a corresponding spacer, such that symmetry is maintained, are used to secure the specimen in the frame and apply a prestress, which is recorded by 120 Ω foil strain gages epoxied to the inside of the biaxial frame.

The structural system providing passive restraint can be modeled as a linear spring with stiffness k^f in series with the test specimen (Fig. 2):

$$k^f = \frac{F_z^f}{u_z^f} \tag{1}$$

where u_z^f is the displacement of the frame and F_z^f is the force applied to the specimen–frame interface. For a linearly elastic specimen with Young's modulus E and Poisson's ratio ν, generalized Hooke's law applies:

$$\sigma_{zz} = E\varepsilon_{zz} + \nu(\sigma_{yy} + \sigma_{xx}) \tag{2}$$

Force equilibrium, $F_z^f = \sigma_{zz}A^s$, between the frame and the specimen gives

$$k^f u_z^f = A^s(E\varepsilon_{zz} + \nu(\sigma_{yy} + \sigma_{xx})) \tag{3}$$

where A^s is the cross-sectional area of the specimen (Fig. 2) perpendicular to the z-axis, the plane strain direction. With perfect contact (no gap or overlap) between the specimen and the frame, specimen deformation u_z^s is equal to the frame deformation:

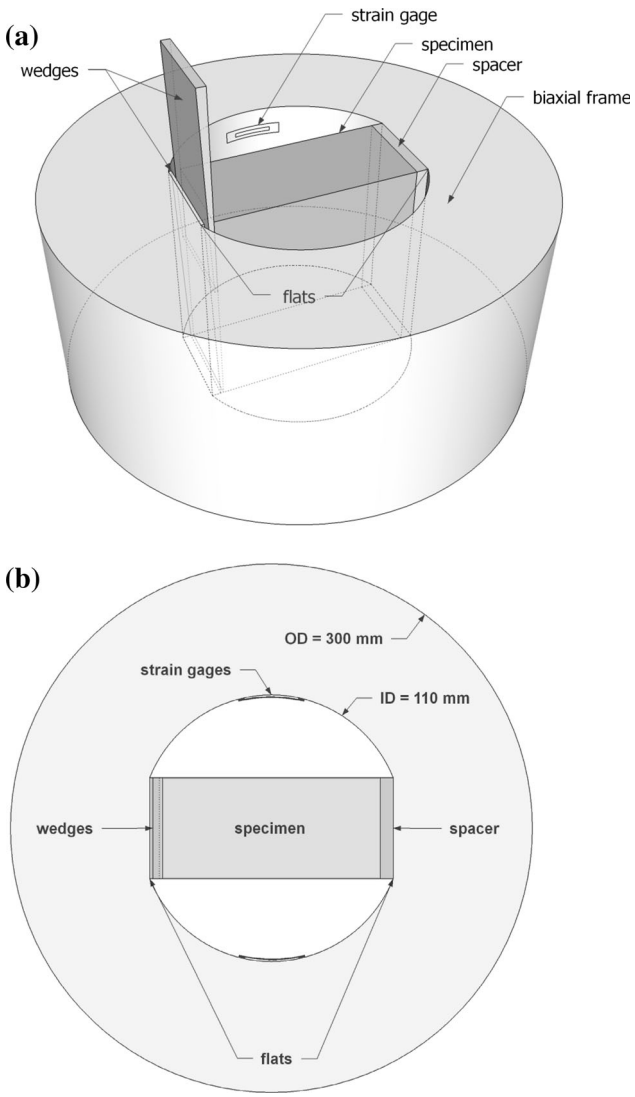

Fig. 1 Biaxial frame and specimen installation: **a** 3D view, **b** Plan view

$$u_z^f = u_z^s = u_z \tag{4}$$

From the definition of $\varepsilon_{zz} = -u_z/w$ (compressive strain positive) and Eq. (3), the displacement u_z can be written as:

$$u_z = \frac{wA^s\nu(\sigma_{yy} + \sigma_{xx})}{k^f w - A^s E} \tag{5}$$

where $2w$ is the width of the specimen.

The principal directions are aligned with the Cartesian coordinates: $\varepsilon_1 = \varepsilon_{yy}$, $\varepsilon_2 = \varepsilon_{zz}$, $\varepsilon_3 = \varepsilon_{xx}$ ($\sigma_1 = \sigma_{yy}$, $\sigma_2 = \sigma_{zz}$, $\sigma_3 = \sigma_{xx}$). The frame restricts ε_2 and thus applies the intermediate principal stress σ_2. Deformation of the frame ε^f is monitored by a set of four tangentially aligned 120 Ω strain gages glued to the inner wall of the biaxial frame (Fig. 1). All strain gages are covered with polyurethane to protect them from the hydraulic oil used for cell pressure.

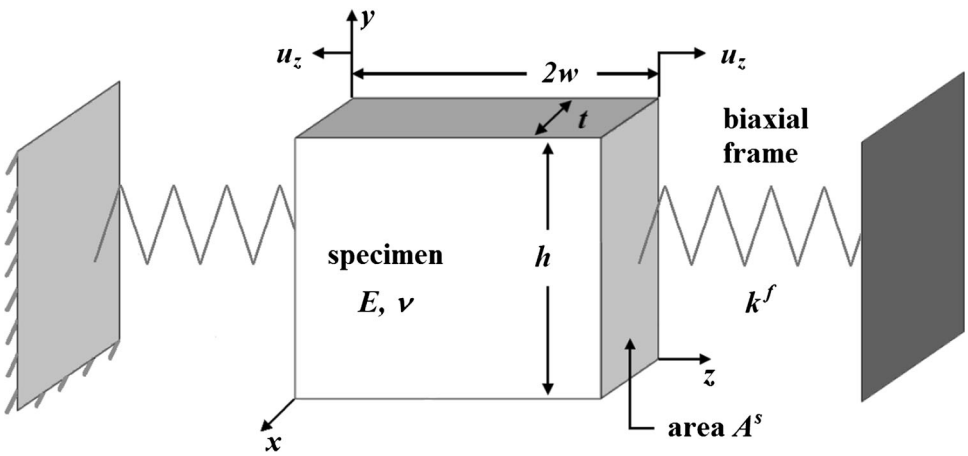

Fig. 2 Mechanical model of biaxial frame and specimen interaction

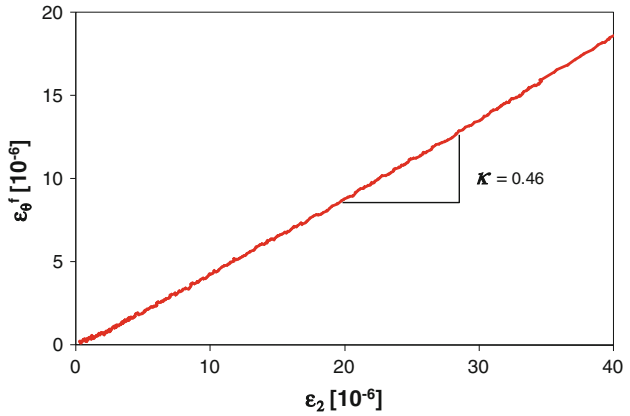

Fig. 3 Relationship between frame strain (ε_θ^f) and specimen strain (ε_2) for the small aluminum specimen at 5 MPa cell pressure

Calibration tests were performed on three specimen sizes referred to as small, medium, and large (height × thickness = 75 × 28, 87 × 44, and 101 × 40 mm with standard width of 100 mm), and three materials: aluminum ($E = 68.9$ GPa, $\nu = 0.33$) for a small size specimen, PMMA ($E = 3.2$ GPa, $\nu = 0.37$) for large and medium sizes, and lead ($E = 15.7$ GPa, $\nu = 0.40$) for medium size. Calibration specimens were instrumented with 120 Ω foil strain gages oriented to measure ε_1 and ε_2. The calibration tests were performed at 0, 5, 10, and 15 MPa cell pressure, and a typical result is shown in Fig. 3; the specimen intermediate strain ε_2 and the deformation of the frame ε_θ^f are linearly related.

The response shown in Fig. 3 can be used to describe the specific strain coefficient of the specimen κ:

$$\kappa(A^s, \sigma_3) = \frac{\varepsilon_\theta^f}{\varepsilon_2} \tag{6}$$

where κ depends on the cross-sectional area of the specimen and cell pressure. Thus, if κ is known, a measure of the plane strain deformation for tests where strain gages on the specimen are not used can be obtained.

The unique relationship, Eq. (6), between the specimen strain ε_2 and the frame strain ε_θ^f for a fixed specimen cross-sectional area A^s and cell pressure σ_3 is used to calculate the strain in the rock specimen. Therefore, with known elastic parameters, Young's modulus E and Poisson's ratio ν, the intermediate principal stress σ_2 can be determined from Eq. (2). Even though inelastic response occurs prior to failure, the elastic parameters in the plane strain direction are not affected appreciably if microcracks form in the x–y plane of the specimen (Carvalho and Labuz 2002); this type of damage has no influence on stiffness in the z-direction. For example, plane strain tests on Berea sandstone were halted at peak stress and unloaded (Riedel and Labuz 2007); these specimens showed a 1–2 % decrease in P-wave velocity in the plane strain direction. During a test performed under constant σ_3 (cell pressure), σ_2 is increasing because of increasing axial stress σ_1 and the frame strain is proportional to ε_2. Passive restraint (the biaxial frame) does not allow the control of the intermediate principal stress, but its value is known and the state of stress is triaxial: $\sigma_1 \neq \sigma_2 \neq \sigma_3$.

2.2 Plane Strain Approximation

Similar to Labuz et al. (1996), the degree of plane strain is defined by the ratio

$$R = -\frac{\varepsilon_2}{\varepsilon_1} \tag{7}$$

The degree of plane strain R has limits from 0 to ν; $R = 0$ means perfect restraint (no deformation in the z-direction), which corresponds to ideal plane strain, and $R = \nu$ means no restraint. With passive restraint, some level of deformation must be realized, as the biaxial frame cannot be infinitely stiff. Substituting expressions for u_z (Eq. 5) and ε_1 (generalized Hooke's law) into Eq. (7) gives

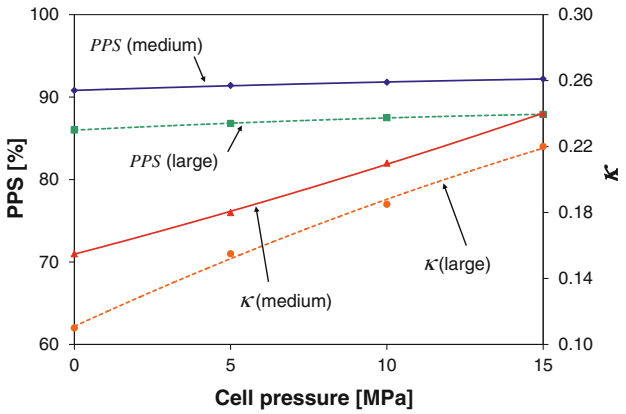

Fig. 4 *PPS* and specific frame stiffness κ as functions of cell pressure for medium and large PMMA specimens

$$R = \frac{\frac{u_z}{w}}{\varepsilon_1} = \frac{\frac{A^s \nu(\sigma_1+\sigma_3)}{k^f w - A^s E}}{\frac{1}{E}(\sigma_1 - \nu(\sigma_2+\sigma_3))} \tag{8}$$

If the frame is soft, then $k^f \to 0$ and $\sigma_2 = 0$:

$$R^{soft} = \frac{\nu(\sigma_1+\sigma_3)}{\sigma_1 - \nu\sigma_3} \tag{9}$$

The degree of restraint is expressed by the percent plane strain (*PPS*):

$$PPS = \left(1 - \frac{R}{R^{soft}}\right) \times 100\ \% \tag{10}$$

A summary of the PMMA calibration tests in terms of *PPS* and κ is shown in Fig. 4, where $A^s = 3{,}830$ mm for the medium size specimen and $A^s = 4{,}040$ mm for the large size specimen. While $PPS = 100$ % is the case of an ideal plane strain condition ($\varepsilon_2 = 0$), it was shown that $PPS > 90$ % is an acceptable approximation (Labuz et al. 1996), and the medium size specimen with $E = 3.2$ GPa satisfies this condition. Figure 4 provides the following observations: *PPS* increases with (i) increasing cell pressure, and (iii) decreasing specimen area A^s.

2.3 Principal Strains

The direction of the major principal stress σ_1 is associated with axial loading, which is measured by upper and lower load cells. Minor principal stress σ_3 is applied by cell pressure (hydraulic oil) and is measured by a pressure transducer. Displacements of the specimen in major (axial) and minor (lateral) principal directions are measured by axial and lateral LVDTs (Fig. 5). However, part of the measured displacement is related to "system" displacement: top and bottom platens attached to the specimen, the internal load cell, and LVDT holders. The system displacement in axial and lateral directions was determined from calibration tests with materials of known elastic properties, such that specimen strains ε_1 and ε_3 can be accurately calculated.

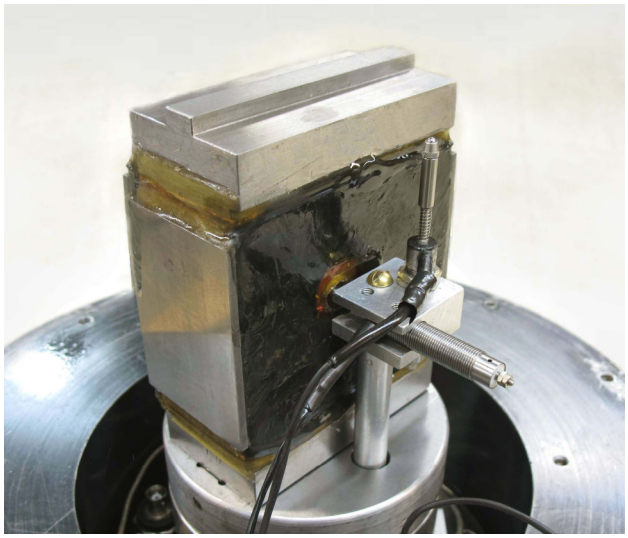

Fig. 5 Photograph of the specimen and LVDTs before it is wedged in the frame

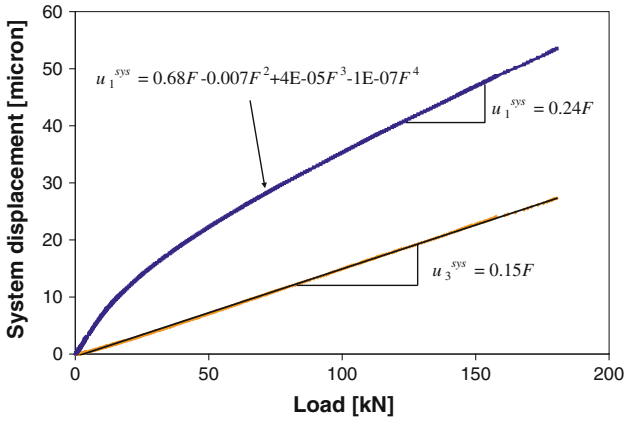

Fig. 6 Calibration of axial and lateral displacement response

The magnitude of axial system displacement u_1^{sys} is

$$u_1^{sys} = u_1^{LVDT} - \varepsilon_1^{gage} h \tag{11}$$

where u_1^{LVDT} and $\varepsilon_1^{gage} h$ are the displacement measured with the axial LVDT and the specimen displacement determined from the axial strain gage, respectively. It was observed that at low axial loads (<30 kN), a fourth order polynomial is the best fit function to characterize the axial system compliance (Fig. 6). However, at higher loads (>30 kN), the dependence of axial system displacement on the load F is linear and can be written as

$$u_1^{sys} = C_A(\sigma_3, A^s)F \tag{12}$$

where $C_A(\sigma_3, A^s)$ is the axial system compliance.

Lateral strain cannot be determined from strain gages, as the surfaces of a specimen parallel with the lateral LVDTs

are in contact with the biaxial frame (Fig. 5), so the lateral specimen strain is calculated with generalized Hooke's law. Lateral displacement of the system is the difference between the elastic lateral displacement of half of the specimen and the average displacement of two lateral LVDTs:

$$u_3^{sys} = u_3^{LVDT} - \varepsilon_3 t/2 \tag{13}$$

The lateral system displacement is found to be linearly related to the load F (Fig. 6). The average lateral compliance $C_L(\sigma_3, A^s)$ is described with

$$u_3^{sys} = C_L(\sigma_3, A^s)F \tag{14}$$

C_A and C_L are calculated to be in the range of 0.23–0.73 micron/kN and 0.14–0.38 micron/kN, respectively; they are found to be decreasing with increasing confining pressure. Also, they are not dependent on the tested material, but increase with increasing specimen size.

3 Experimental Results

3.1 Indiana Limestone Properties

To demonstrate the utility of the apparatus, Indiana limestone, a sedimentary rock with grain size less than 1 mm, was selected for plane strain and conventional triaxial compression/extension testing. A single block, 225 × 215 × 200 mm (x, y, z-axes), with density $\rho = 2{,}300$ kg/m^3 and porosity $n = 13$ %, was used to fabricate all specimens. Ultrasonic velocity measurements show that the rock has a low level of anisotropy (<3 %). P-wave and S-wave velocities (V_p [km/s], V_s [km/s]) in x, y, and z-directions were measured to be (4.23, 2.53), (4.39, 2.54), and (4.29, 2.51). Thus, the rock is assumed to be elastically isotropic.

Uniaxial compression tests were performed on four right circular cylinders (cores), and conventional triaxial compression/extension tests were performed on ten cores; all specimens were prepared in accordance with ISRM standards (Brown 1981) and loaded at an axial displacement rate of 5×10^{-4} mm/s. For the uniaxial tests, axial and tangential strains were monitored by foil strain gages to determine Young's modulus E and Poisson's ratio ν within the linear response of the rock, typically from 10 to 50 % of the uniaxial compression strength (UCS). The cylindrical specimens were 31.5 mm in diameter, which is smaller than the suggested diameter size of 54 mm, but the diameter to grain size ratio is still larger than the recommended value of 10:1. The height of the cylindrical specimens ranged from 82 to 90 mm, within the desired height to diameter ratio of 2–3. The ends of the specimens were lubricated with stearic acid (Labuz and Bridell 1993). The results of the uniaxial tests yielded the following range of the parameters: UCS = 42–44 MPa, E = 26–29 GPa, and ν = 0.19–0.21.

3.2 Prismatic Specimens

Three plane strain compression experiments, BXIL-1, BXIL-2, and BXIL-3 were conducted at 0, 5, and 10 MPa cell pressures, respectively. Three small prismatic specimens (100 × 75 × 28 mm) were cut from the block in the same way as the core specimens, i.e., bedding aligned normal to the axial stress (y-direction in Fig. 2). For each specimen, all of the faces were ground so that opposite sides were parallel and adjacent sides were perpendicular within ±0.01 mm in 100 mm. The specimen was assembled with the upper and lower steel platens contacting the 100 × 28 mm faces and two steel plates, 3 mm thick, contacting the 28 × 75 mm faces. The four surfaces in contact with polished-steel platens were covered with stearic acid to reduce friction at the platen–specimen interfaces and promote homogeneous deformation (Labuz and Bridell 1993). The specimen and platens were held together in a custom jig and two specimen sides exposed to the cell pressure were sealed by a polyurethane coating (Fig. 5).

The specimen with attached platens was wedged in the frame so that the stress in the plane strain direction (z-axis) was at least 10 % greater than the cell pressure σ_3; the frame strain was measured during the wedging process. The entire biaxial frame was placed inside the pressure cell and exposed to fluid pressure during an experiment. The cell was filled with hydraulic oil and the pressure was applied with a microprocessor-based hydraulic pump that maintained cell pressure at a constant value, within a tolerance of 0.1 MPa. Closed-loop, servo-controlled tests were performed within a 1,000 kN load frame (MTS Systems, Eden Prairie, MN) with an average lateral displacement rate of 5×10^{-5} mm/s as a feedback signal. A cell pressure-compensated load cell, with a sensitivity of 5 kN/mV/vdc, was placed below the specimen, between the lower loading platen and the base unit, and provides an accurate measurement of axial load. *PPS* was calculated to be 84.7 % ($\sigma_3 = 0$ MPa), 87.5 % ($\sigma_3 = 5$ MPa), and 90.2 % ($\sigma_3 = 10$ MPa); recall that PPS increases with increasing cell pressure for the specimens of the same size and elastic parameters. Only the test conducted at 10 MPa (BXIL-3) satisfied $PPS > 90$ %, and its results are analyzed in terms of elastic and inelastic material response.

3.3 Elastic Response

The incremental behavior of an isotropic linearly elastic solid in plane strain takes the following form for principal strains and stresses ($\varepsilon_2 = 0$):

$$\Delta\varepsilon_1 = \frac{1+v}{E}[(1-v)\Delta\sigma_1 - v\Delta\sigma_3]$$
$$\Delta\varepsilon_3 = \frac{1+v}{E}[(1-v)\Delta\sigma_3 - v\Delta\sigma_1] \quad (15)$$
$$\Delta\sigma_2 = v(\Delta\sigma_1 + \Delta\sigma_3)$$

Noting that cell pressure is constant throughout the test ($\Delta\sigma_3 = 0$) and taking the sign convention of compression positive, Young's modulus E and Poisson's ratio v are

$$E = \Delta\sigma_1 \frac{\Delta\varepsilon_1 - 2\Delta\varepsilon_3}{(\Delta\varepsilon_1 - \Delta\varepsilon_3)^2} \quad (16)$$

$$v = \frac{-\Delta\varepsilon_3}{\Delta\varepsilon_1 - \Delta\varepsilon_3} \quad (17)$$

Using the system corrections for axial and lateral displacements, the increments of principal strains $\Delta\varepsilon_1$ and $\Delta\varepsilon_3$, as well as the increment of axial stress $\Delta\sigma_1$, were calculated in the range of linear response (10–50 % peak axial load), producing the values of Young's modulus $E = 28.0$ GPa and Poisson's ratio $v = 0.21$, which are close to those measured in the uniaxial compression tests.

3.4 Inelastic Response

Permanent volume change, both compaction and dilation, has been noted for a wide variety of rock when stressed beyond an elastic limit (Brace et al. 1966). To observe inelastic response, elastic compaction and distortion must be removed from the total deformation.

For plane (biaxial) deformation, volume strain ε and shear strain γ are written as:

$$\varepsilon = \varepsilon_1 + \varepsilon_3 \quad (18)$$

and

$$\gamma = \varepsilon_1 - \varepsilon_3 \quad (19)$$

Total volume strain and the axial stress difference for BXIL-3 test are plotted as a function of axial strain (Fig. 7), and show typical behavior of a dilatant rock. Using compression positive sign convention, the volume strain increased due to compaction of the specimen, and then decreased as the rock dilates. The onset of the nonlinear volume strain response was used as indicating the state when inelastic (plastic) deformation initiated.

The plastic strains were determined by removing the calculated elastic response from the measured deformation assuming no change in elastic parameters:

$$d\varepsilon^p = d\varepsilon^{meas} - d\varepsilon^e \quad (20)$$

$$d\gamma^p = d\gamma^{meas} - d\gamma^e \quad (21)$$

For the test conducted at 10 MPa cell pressure, plastic deformation was associated with a small amount of plastic

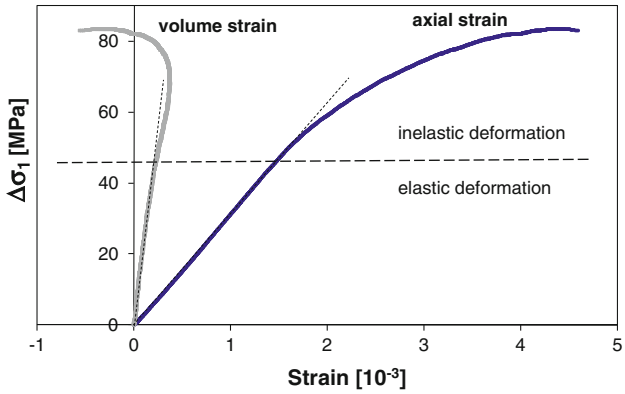

Fig. 7 Axial and volume strain response for plane strain compression test

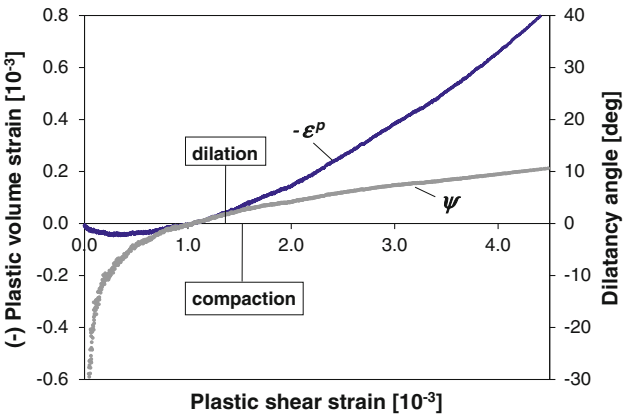

Fig. 8 Dilatancy behavior for BXIL-3 test: $-\varepsilon^p$ and ψ versus γ^p

compaction followed by a dilatant response (Fig. 8). The increase of plastic volume strain was fairly linear near peak axial load, with the plastic shear strain at peak $\gamma^p = 4.5 \times 10^{-3}$. The dilatancy angle ψ (Hansen 1958) is defined by

$$\sin\psi = -\frac{d\varepsilon^p}{d\gamma^p} \quad (22)$$

As displayed in Fig. 8, the compactive behavior of Indiana limestone at the onset of plastic deformation is observed as a negative dilatancy angle, and plastic compaction is followed by a dilatant response shown as a positive dilatancy angle, which increases with plastic shear strain to 11° at peak axial load.

3.5 Strength

The results of three plane strain compression experiments can be compared with the results of the conventional triaxial tests in terms of principal stresses at failure. A linear strength relation that includes the intermediate stress is the Paul-Mohr-Coulomb (PMC) failure criterion (Paul 1968):

Table 1 Principal stresses at failure for plane strain compression and triaxial compression and extension experiments

Test name	σ_1 [MPa]	σ_2 [MPa]	σ_3 [MPa]
BXIL-1	45.4	8.4	0.0
BXIL-2	61.2	16.8	5.0
BXIL-3	101.0	26.4	10.0
Triax-comp-1	69.7	5.0	5.0
Triax-comp-2	82.2	10.0	10.0
Triax-comp-3	103.1	15.0	15.0
Triax-comp-4	100.8	20.0	20.0
Triax-comp-5	114.8	25.0	25.0
Triax-comp-6	133.2	30.0	30.0
Triax-ext-1	50.0	50.0	0.7
Triax-ext-2	58.0	58.0	2.6
Triax-ext-3	60.0	60.0	1.7
Triax-ext-4	62.0	62.0	2.1

$$A\sigma_1 + B\sigma_2 + C\sigma_3 = 1 \tag{23}$$

where

$$\begin{aligned} A &= (1 - \sin\phi_c)/(2V_o \sin\phi_c) \\ B &= (\sin\phi_c - \sin\phi_e)/(2V_o \sin\phi_c) \\ C &= -(1 + \sin\phi_e)/(2V_o \sin\phi_e) \end{aligned} \tag{24}$$

Three material parameters, friction angles in compression ϕ_c and extension ϕ_e, and the uniform triaxial tensile strength V_o, can be identified from conventional triaxial compression and extension experiments and are sufficient to define a six-sided failure surface (Meyer and Labuz 2013).

Of the ten triaxial tests, six were performed in compression with $\sigma_1 = \sigma_{axial}$ and $\sigma_2 = \sigma_3 = \sigma_{radial}$, and four in extension with $\sigma_1 = \sigma_2 = \sigma_{radial}$ and $\sigma_3 = \sigma_{axial}$. The compression tests were conducted as loading tests, where $\sigma_{axial}$is increased ($\Delta\sigma_{axial} > 0$) from $\sigma_{axial} = \sigma_{radial}$ until failure and σ_{radial} = constant. The remaining four triaxial specimens were tested in extension unloading, with σ_{axial} decreasing ($\Delta\sigma_{axial} < 0$) from $\sigma_{axial} = \sigma_{radial}$ until failure and σ_{radial} = constant. The results from the compression and extension experiments, as well as the results of plane strain compression tests, are presented in Table 1.

For the axisymmetric stress state in conventional triaxial testing, the stress invariants p and q are:

$$p = \frac{\sigma_1 + \sigma_2 + \sigma_3}{3} = \frac{\sigma_{axial} + 2\sigma_{radial}}{3} \tag{25}$$

and

$$q = \sqrt{3J_2} = \sigma_{axial} - \sigma_{radial} \tag{26}$$

where J_2 is the second invariant of the stress deviator $S_{ij} = \sigma_{ij} - p\delta_{ij}$ and δ_{ij} = Kronecker delta. The PMC failure criterion in compression can be written as

$$q = \frac{6\sin\varphi_c}{3 - \sin\varphi_c} p + \frac{6c_c \cos\varphi_c}{3 - \sin\varphi_c} \tag{27}$$

The extension line can be given in a similar manner:

$$q = -\frac{6\sin\varphi_e}{3 - \sin\varphi_e} p - \frac{6c_e \cos\varphi_e}{3 - \sin\varphi_e} \tag{28}$$

where c_c and c_e are the cohesion in compression and extension, respectively (Meyer and Labuz 2013).

The compression and extension data were fitted with lines that intersect the p-axis at the same point V_o, which is required for any failure surface. The corresponding lines of best fit with a common vertex were determined by finding the maximum value of the sum of the correlation coefficients ($R_c^2 + R_e^2$), under the condition that the absolute value of the difference $|R_c^2 - R_e^2|$ is a minimum (Meyer and Labuz 2013. The data and the best fit lines with the constraint of the same V_o are shown in Fig. 9a ($R_c^2 = R_e^2 = 0.926$).

Using Eqs. (27) and (28), a difference in friction angles in compression and extension is observed: ϕ_c = 32.1° and

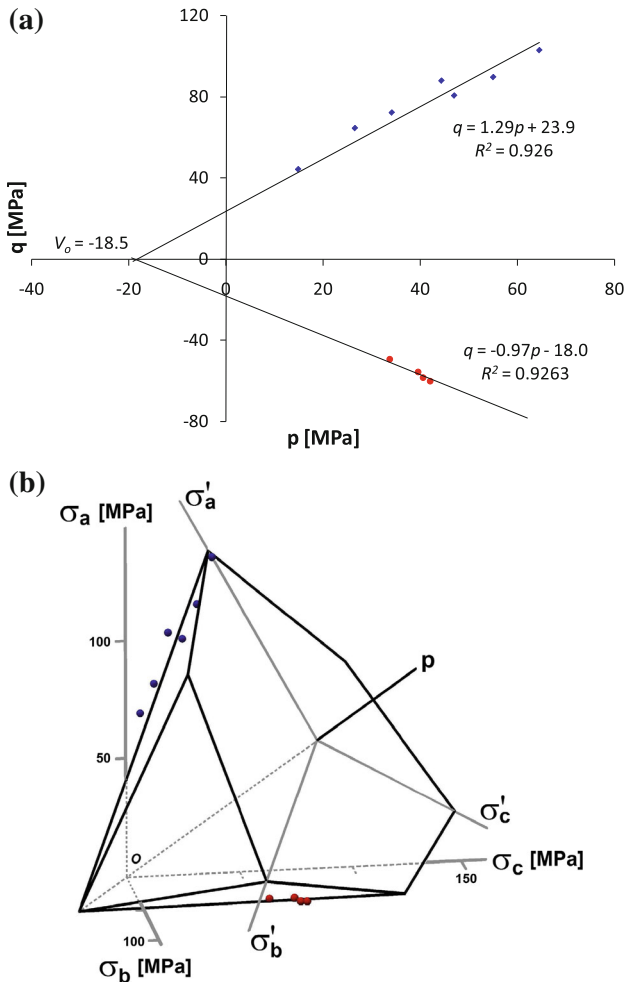

Fig. 9 Results of triaxial compression (*blue dots*) and extension (*red dots*) tests in the **a** p–q plane and **b** principal stress space (color figure online)

$\phi_e = 35.4^\circ$, which is a sufficient, but not necessary condition for a material exhibiting an intermediate stress effect. For isotropic rock, knowledge of the two internal friction angles ϕ_c and ϕ_e, and one strength parameter such as the vertex V_o is sufficient to define a six-sided failure surface in the principal stress space σ_a, σ_b, σ_c, with no order implied (Fig. 9b); the data from the conventional triaxial tests are shown. The hexagonal pyramid results for the six combinations of the ordering of the principal stresses.

The data from the plane strain experiments can be presented in principal stress space (Fig. 10a) and on a plane perpendicular to the p-axis ($\sigma_a = \sigma_b = \sigma_c$) called the π-plane and described by $p =$ constant; the intersection of the failure surface and the π-plane is a hexagon that displays a three-fold symmetry (Fig. 10b). Note that for conventional triaxial tests $\sigma_a' = q$, where σ_a', σ_b', and σ_c' are the projections of σ_a, σ_b, and σ_c on the π-plane. The results of the three plane strain compression tests (BXIL-1, BXIL-2, and BXIL-3) and the π-planes at failure are presented in Fig. 10a, b. The specimen tested at $\sigma_3 = 10$ MPa failed at a higher major principal stress σ_1 than predicted by the PMC criterion, but the data points for the specimens at 0 and 5 MPa cell pressure (BXIL-1 and BXIL-2) are consistent with the six-sided failure surface obtained from the conventional triaxial tests.

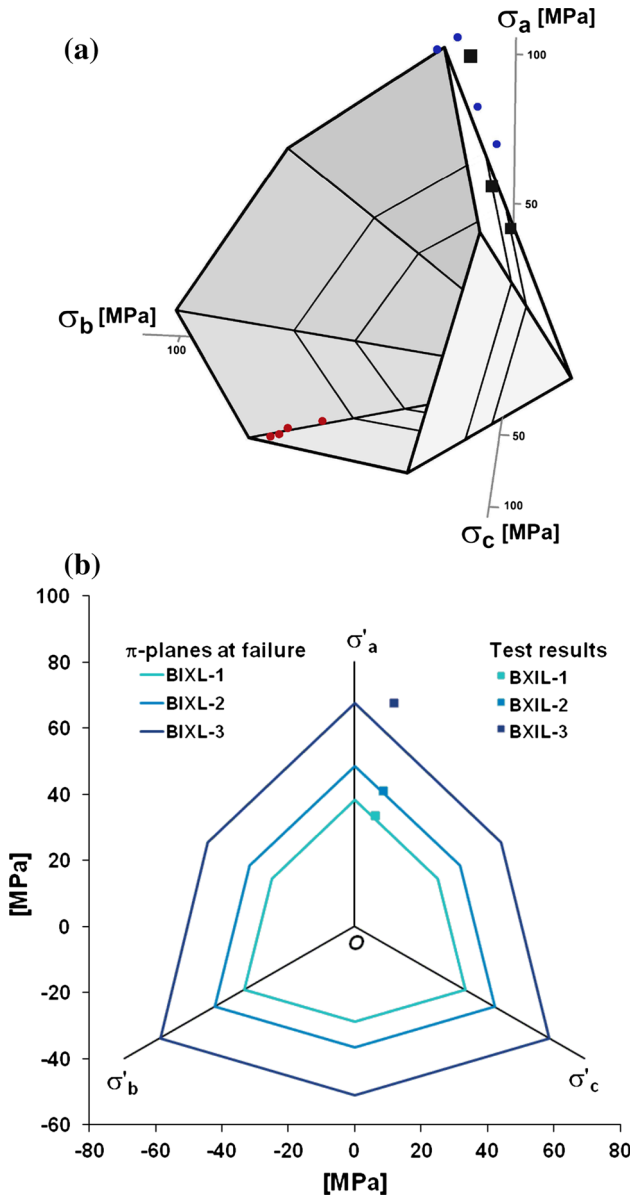

Fig. 10 Plane strain test (BXIL-1, BXIL-2, and BXIL-3) results with the **a** failure surface and triaxial data and **b** corresponding π-planes

4 Conclusions

Passive restraint provides a simple method to achieve plane strain, although calibration and assumed linear response are needed to determine the value of the intermediate stress, which differs from the major and minor principal stresses. Biaxial deformation allows one to measure accurately the in-plane strains, and to evaluate the elastic and inelastic parameters of a rock.

To demonstrate the utility of passive restraint, Indiana limestone was tested using standard axisymmetric loading and plane strain compression. The material parameters, both deformation- and stress-based, compared well: Poisson's ratio ν and Young's modulus E measured in plane strain loading were in the range of those obtained from uniaxial compression. From the plane strain test, plastic volume and shear strains showed that, for the specimen tested at $\sigma_3 = 10$ MPa, the compactive behavior of rock at the onset of plastic deformation was followed by a dilatant response, with the dilatancy angle increasing with plastic shear strain and being equal to 11° at failure, much less than the compression friction angle of 32°. Comparison of the principal stresses at failure with the Paul-Mohr-Coulomb failure surface confirmed the effect of the intermediate principal stress on strength. The friction angle measured in conventional triaxial extension tests was larger than the one measured from compression tests, a sufficient but not necessary condition of the intermediate stress effect, and the strength data from the plane strain tests were consistent.

Acknowledgments Partial support was provided by DOE grant DE-FE0002020 funded through the American Recovery and Reinvestment Act. Mr. Jim Meyer and Dr. Chu-Shu Kao assisted with the experiments; Mr. Justice Harvieux helped with the figures.

References

Al-Hussaini MM (1968) The behavior of sand under plane strain conditions. Ph.D. dissertation, Georgia Institute of Technology

Bésuelle P, Hall SA (2011) Characterization of the strain localization in a porous rock in plane strain condition using a new true-triaxial apparatus. In: Bonelli S, Dascalu C, Nicot F (eds) Advances in bifurcation and degradation in geomaterials. Springer, pp 345–352

Brace WF, Paulding BW, Scholz C (1966) Dilatancy in the fracture of crystalline rocks. J Geophys Res 71(16):3939–3953

Brown ET (1981) Rock characterization, testing and monitoring: ISRM suggested methods. International Society for Rock Mechanics, Pergamon Press

Campanella RG, Vaid YP (1973). Influence of stress path on the plane strain behavior of sensitive clay. Proc 8th Int Conf Soil Mech Found Engng 1: 85–92

Carvalho F, Labuz JF (2002) Moment tensors of acoustic emission in shear faulting under plane-strain compression. Tectonophysics 356:199–211

Cornforth DH (1964) Some experiments on the influence of strain conditions on the strength of sand. Geotechnique 14(2):143–167

Drescher A, Vardoulakis I, Han C (1990) A biaxial apparatus for testing soils. Geotech Testing J ASTM 13:226–234

Duncan JM, See HB (1966) Strength variation along failure surface in clay. Proceedings ASCE 92(SM6):81–104

Franklin JA, Hoek E (1970) Developments in triaxial testing technique. Rock Mech 2:223–228

Haimson B (1978) The hydrofracturing stress measuring method and recent field results. Int J Rock Mech Min Sci Geomech Abstr 15(4):167–178

Haimson B, Chang C (2000) A new true triaxial cell for testing mechanical properties of rock, and its use to determine rock strength and deformability of westerly granite. Int J Rock Mech Min Sci 37:285–296

Hansen B (1958) Line ruptures regarded as narrow rupture zones: basic equations based on kinematic considerations. In: Conf Earth Pressure Problems, Brussels, Belgium, 1. pp 39–49

Henkel DJ, Wade NH (1966) Plane strain tests on a saturated remolded clay. J Soil Mech Found Engng ASCE 92(SM6):67–80

Jaeger JC, Cook NGW, Zimmerman RW (2007) Fundamentals of Rock Mechanics, 4th edn. Blackwell, London

Kjellman W (1936) Report on an apparatus for consummate investigation of the mechanical properties of soil. Proc 1st Int Conf Soil Mech Found Engng II, 16–20

Labuz JF, Bridell JM (1993) Reducing frictional constraint in compression testing through lubrication. Int J Rock Mech Min Sci Geomech Abstr 30:451–455

Labuz JF, Dai ST, Papamichos E (1996) Plane-strain compression of rock-like materials. Int J Rock Mech Min Sci Geomech Abstr 33:573–584

Leussink H, Wittke W (1963) Difference in triaxial and plane strain shear strength. ASTM Special Publication No. 361: 77–89

Marsal RJ, DeArellano LR, Nunez GA (1967) Plane strain testing of rockfill materials. Proc 3rd Pan-American Conf Soil Mech Found Engng 1: 249–270

Meyer JP, Labuz J (2013) Linear failure criteria with three principal stresses. Int J Rock Mech Min Sci 60:180–187. doi:10.1016/j.ijrmms.2012.12.040

Mogi K (1967) Effect of the intermediate principal stress on rock failure. J Geophys Res 72:5117–5131

Paul B (1968) Generalized pyramidal fracture and yield criteria. Int J Solids Struct 4:175–196

Riedel JJ, Labuz J (2007) Propagation of a shear band in sandstone. Int J Numer Anal Meth Geomech 31:1281–1299

Smith IM (1963) An investigation of the strength characteristics of soft clay under condition of plane strain. Graduate research report, University of California, Berkeley

Vardoulakis IG, Goldscheider M (1981). Biaxial apparatus for testing shear bands in soils. Proc 10th Int Conf Soil Mech Found Engng, Stockholm, 819–824

Wawersik WR, Carlson LW, Holcomb DJ, Williams RJ (1997) New method for true-triaxial rock testing. Int J Rock Mech Min Sci 34:330